Ultrabroadband lattice filters for integrated photonic spectroscopy and sensing

Nathan F. Tyndall
Todd H. Stievater
Dmitry A. Kozak
Marcel W. Pruessner
Scott A. Holmstrom
William S. Rabinovich

SPIE.

Ultrabroadband lattice filters for integrated photonic spectroscopy and sensing

Nathan F. Tyndall,[a,*] Todd H. Stievater,[a] Dmitry A. Kozak,[a] Marcel W. Pruessner,[a] Scott A. Holmstrom,[b] and William S. Rabinovich[a]

[a]Naval Research Laboratory, Optical Sciences Division, Washington, DC, United States
[b]University of Tulsa, Department of Physics and Engineering Physics, Tulsa, Oklahoma, United States

Abstract. We report the design, fabrication, and measurement of waveguide lattice filters for use in integrated Raman- or fluorescence-based spectroscopy and sensing systems. The filters consist of a series of broadband directional couplers and optical delay sections that create an n-stage unbalanced Mach–Zehnder interferometer specifically designed to segregate pump light and redshifted signal light in the two output ports. We first report the design criteria for optimal filter performance. Then, we use these criteria with numerical beam propagation methods to design specific broadband couplers. The filters were fabricated by a photonic integrated circuit foundry and measured using white-light spectroscopy. We report both four-stage and eight-stage filters, with the eight-stage filter demonstrating a 190-nm-wide signal passband (1100 cm^{-1}) on the "through" port with <1.5 dB of ripple and a 17-nm-wide, 20-dB extinction band at the filter resonance. © *The Authors. Published by SPIE under a Creative Commons Attribution 3.0 Unported License. Distribution or reproduction of this work in whole or in part requires full attribution of the original publication, including its DOI.* [DOI: 10.1117/1.OE.57.12.127103]

1 Introduction

Waveguide-based spectroscopic sensors can detect and identify vapor- or liquid-phase analytes on a chip-scale photonic platform. For example, the detection of biological monolayers,[1] liquids,[2] and trace concentrations of toxic vapors[3] have been demonstrated with waveguide-enhanced Raman spectroscopy. Fluorescence spectroscopy using the evanescent field above nanophotonic waveguides has also been demonstrated for biological sensing.[4–6] A fully integrated sensing system would be miniature, lightweight, and low-power but requires the integration of the laser source as well as the development of on-chip, broadband, wavelength-selective components such as spectrometers and optical filters.

A number of on-chip interferometric waveguide filters exist, including microring resonators,[7] arrayed-waveguide gratings,[8,9] and unbalanced Mach–Zehnder interferometers.[10] In addition, adiabatic mode-evolution waveguides have also recently been shown to act as edge filters in the c-band.[11] However, since Raman and fluorescence spectroscopy demand high-extinction, narrow spectral features with very large adjacent optical passbands (e.g., a Stokes shift of 1500 cm^{-1} from a 1300-nm pump corresponds to a signal wavelength of 1600 nm), only filters with a large free-spectral range (FSR) are useful. In this work, we show that multistage unbalanced Mach–Zehnder interferometers, also known as lattice filters (LFs), can meet this requirement and serve as both input and output filters for sensing and spectroscopy, as shown schematically in Fig. 1(a). We describe the design, fabrication, and measurement of four-stage and eight-stage low-loss LFs in silicon nitride (SiN) waveguides. Our

measured filter passband of 190 nm is the largest reported in a photonic integrated circuit filter.

2 Filter Design

One-dimensional photonic LFs[10,12,13] are based on an n-stage sequence of four-port interferometric filters connected in series. Here, a single stage consists of a broadband four-port directional coupler (DC) followed by a differential delay (DD) section, as shown schematically in Fig. 1(b). After the last stage, a final DC is used to create an n-stage unbalanced Mach–Zehnder interferometer. Each stage of the n-stage LF described in this work is identical.

LFs can be modeled using a transfer matrix approach in which a 2×2 matrix relates the optical fields at the two input ports to those at the output ports, each represented by 2×1 column vectors. The transfer matrix for a general DC is given as

$$S^{DC} = \begin{bmatrix} \tau_1 & -i\kappa \\ -i\kappa & \tau_2 \end{bmatrix}, \tag{1}$$

where $|\tau_1|^2 = |\tau_2|^2 = |\tau|^2$ is the "through" power coupling coefficient, $|\kappa|^2$ is the "cross" power coupling coefficient with $|\kappa|^2 = 1 - |\tau|^2$. These complex coupling coefficients depend strongly on the physical properties of the DC and contain phase information that may differ between the top path ("1") and the bottom path ("2") due to different optical path lengths within the coupler.

The transfer matrix for a DD section is given as

$$S^{DD} = \begin{bmatrix} e^{-i\beta\Delta L} & 0 \\ 0 & 1 \end{bmatrix}, \tag{2}$$

where ΔL is the differential path length of the DD and $\beta = 2\pi n_{\text{eff}}/\lambda$ is the waveguide propagation constant for

*Address all correspondence to: Nathan F. Tyndall, E-mail: nathan.tyndall@nrl.navy.mil

the design mode, where λ is the free space wavelength and n_{eff} is the effective index of the waveguide mode.

The transfer matrix for a complete n-stage LF is found by multiplying the matrices for each component, which includes $(n + 1)$ DCs and n DD sections

$$S^{LF} = S^{DC} \prod_{j=1}^{n} S_j^{DD} S_j^{DC}. \quad (3)$$

Optimal performance is achieved by coordinating the DC coupling and DD differential phase shift for maximum extinction on the through port at the desired primary filter resonance while maximizing the FSR. With the DDs designed to ensure differential phase shifts per stage equal to an integer multiple of 2π at the primary filter resonance, the DCs are designed to provide the appropriate coupling at this wavelength. On resonance, the LF response is equivalent to $(n + 1)$ symmetric DCs connected directly in series, and Eq. (3) can be written

$$\begin{bmatrix} |\tau| & -i|\kappa| \\ -i|\kappa| & |\tau| \end{bmatrix}^{(n+1)} = \begin{bmatrix} \cos((n+1)\theta) & -i\sin((n+1)\theta) \\ -i\sin((n+1)\theta) & \cos((n+1)\theta) \end{bmatrix}, \quad (4)$$

where $\theta = \arctan(\sqrt{1 - |\tau|^2}/|\tau|)$. Optimal coupling for light entering a single input port of the LF is then given by setting the diagonal elements of Eq. (4) to zero

$$\cos\left[(n + 1)\arctan\left(\sqrt{1 - |\tau|^2}/|\tau|\right)\right] = 0. \quad (5)$$

For a four-stage LF, this yields $|\tau|^2 = 0.905$ and for an eight-stage LF, $|\tau|^2 = 0.970$.

The transfer matrix method was used to numerically simulate the response of dispersionless LFs (n_{eff} and τ independent of λ) with total differential optical path length differences per stage equal to 6.5 μm. The results for four- and eight-stage filters are shown in Figs. 1(c) and 1(d),

respectively. As can be seen in the figure, an ideal eight-stage filter would completely block a 1.3-μm pump in the through port and block the signal in the cross port by >10 dB over most of the 300-nm FSR while passing the pump in the cross port over an effective bandwidth of ~20 nm and passing the signal in the through port with <1 dB ripple over 280 nm. For integrated fluorescence or Raman applications, the advantages of a higher-order filter are clear: better pump extinction, flatter passband, and narrower filter resonance. However, higher-order filters are more sensitive to fabrication nonuniformities and occupy more space.

Traditional symmetric DCs with straight, parallel, adjacent waveguides interacting over fixed distances have coupling coefficients that depend strongly on wavelength over the broad wavelength regions needed for fluorescence and Raman spectroscopy. However, relatively flat coupling over large optical bandwidths has been demonstrated using an asymmetrical coupler.[14–16] Here, we have followed the approach described by Lu et al.[16] in designing both 90/10 and 97/3 broadband DCs in a SiN/SiO$_2$ (core/cladding) waveguide platform for the TE$_{00}$ mode.

An asymmetric coupler is shown schematically in Fig. 2 and consists of two waveguides feeding three closely spaced sections: the first and third are symmetric coupling sections, both with length L_1 and waveguide widths $w = 1.2$ μm;
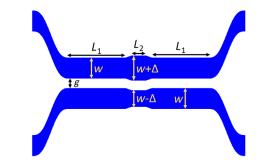

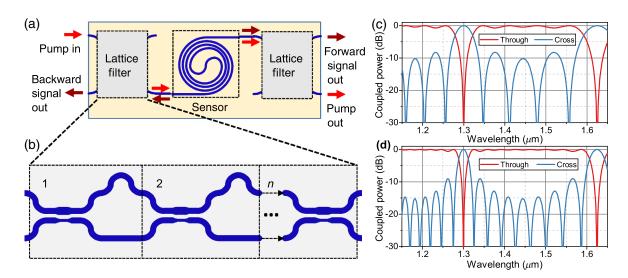**Fig. 2** Schematic of a broadband asymmetric DC (not to scale).

Fig. 1 (a) System design for a PIC transducer with integrated broadband filters. (b) An n-stage LF comprising n unbalanced propagation stages and $n + 1$ broadband DCs. (c) The calculated response of a four-stage LF with optimized coupling. (d) The calculated response of an eight-stage LF with optimized coupling.
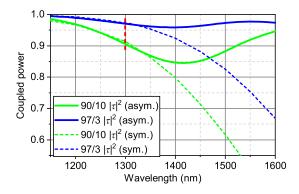
Fig. 3 Simulated through coupling $|\tau|^2$ for the 90/10 and 97/3 DCs. The solid lines correspond to the broadband asymmetric DC, whereas the dashed lines correspond to a symmetric DC, shown for reference (see text). The red line indicates the filter resonance wavelength of 1300 nm.

Fig. 4 Measured through-coupling spectra of the 90/10 and 97/3 broadband DCs. The red dashed line indicates 90.5% and 97.0% coupling, respectively.

the second is a phase control section with length L_2 and waveguide widths $w + \Delta$ (top arm) and $w - \Delta$ (bottom arm), where $\Delta = 0.3$ μm. The sections are connected by 10 μm-long tapered sections. The gap between the waveguides, $g = 1.0$ μm, is kept constant over all three sections. The device was modeled using *PhoeniX OptoDesigner* two-dimensional beam propagation simulations and optimized for uniform coupling from 1150 to 1600 nm for the TE_{00} mode.

The design parameters that give 90.5% through-coupling at 1300 nm while also minimizing deviations from this coupling over a full FSR are: $L_1 = 96$ μm and $L_2 = 12$ μm. For 97.0% through-coupling, we found $L_1 = 82$ μm and $L_2 = 10$ μm. The calculated through-coupling $|\tau|^2$ for each coupler using these parameters is shown in Fig. 3. The deviation from 97% coupling of the 97/3 coupler is less than 3% over this wavelength range, and the deviation from 90% coupling of the 90/10 coupler is less than 10%. Also shown for reference in Fig. 3 is the calculated through coupling of a symmetric DC with no tapers, $L_1 = L_2 = 0$, $w = 1.2$ μm, and gaps of 0.53 and 0.72 μm for 90/10 and 97/3 coupling, respectively, at 1300 nm. The minimum bend radius for all devices is 150 μm.

We also used *PhoeniX OptoDesigner* to determine the wavelength dependence of n_{eff} for the 1.2 μm wide waveguide in the DD stage to determine the appropriate differential length for the filter resonance at 1300 nm: $\Delta L = 3.22$ μm was used for both the four-stage and eight-stage filters.

3 Fabrication and Measurement

The 90/10 and 97/3 broadband DCs were laid out as individual components and as part of a four-stage or eight-stage LF, respectively. They were connected to edge couplers and fabricated in the SiN waveguide layer as part of a multiproject wafer run at AIM Photonics.[17]

We used lensed optical fibers made from PM980-XP polarization maintaining fiber (Oz Optics) to couple white light into the quasi-TE waveguide modes. The white light source is a temperature-stabilized tungsten blackbody emitter (Thorlabs SLS201L) that was linearly polarized and focused into the optical fiber. Emitted light from the waveguide was collected by a second lensed fiber and sent to a 1/2-m spectrometer for detection by a liquid-nitrogen
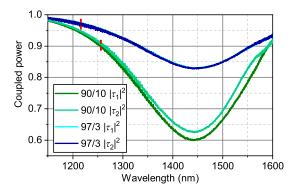
cooled InGaAs photodiode array (Princeton Instruments SP-2500 and Pylon-IR).

For each component, four measurements were made, corresponding to excitation from each input port and collection via each output port. The measured spectra were normalized by the sum of the output spectra for excitation through a common input port so that overall filter losses are not reflected in the spectra shown. Subsequent measurements that compare the filter transmission to a straight waveguide with identical edge couplers indicate that the overall filter losses are less than the 1 to 2 dB uncertainty in the coupling loss.

The measured through couplings ($|\tau_1|^2$ and $|\tau_2|^2$) of the broadband DCs are shown in Fig. 4. Slight differences between $|\tau_1|^2$ and $|\tau_2|^2$ reflect the experimental coupling error. Overall, both couplers show a stronger wavelength dependence than our models predict (compare to Fig. 3), as well as a stronger overall cross-coupling. This results in an optimal coupling fraction (indicated by the red tick mark on each plot) that is blueshifted for each coupler compared to our models. The origin of this discrepancy is unclear but is likely related to a difference between the actual material parameters and those that we used in our models.

The measured through coupling ($|S_{11}^{\text{LF}}|^2$ and $|S_{22}^{\text{LF}}|^2$) and cross-coupling ($|S_{21}^{\text{LF}}|^2$ and $|S_{12}^{\text{LF}}|^2$) of the four-stage and eight-stage LFs are shown in Figs. 5 and 6, respectively. As with the spectra from the broadband DC, the LF spectra are normalized to the total power from both output ports.
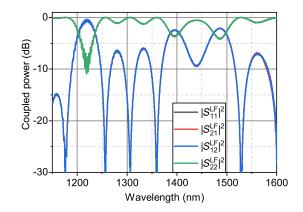

Fig. 5 Measured through- and cross-coupling spectra of the four-stage LF.
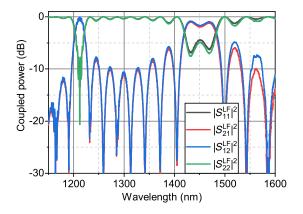
Fig. 6 Measured through- and cross-coupling spectra of the eight-stage LF.

Both LFs are characterized by a resonance that is blueshifted compared to the design wavelength. This shift is due to DC modeling uncertainties as well as the same fabrication discrepancy that results in the excess cross-coupling shown in Fig. 4. This fabrication discrepancy impacts the phase delay of the DC and results in different filter resonances for the two DC designs. The four-stage filter shows 10-dB extinction at the resonance, which is significantly blueshifted from the design wavelength. The mismatch between the filter resonance (1220 nm) and the optimal coupling (1255 nm) results in the relatively poor extinction. The eight-stage filter shows 20-dB extinction at the filter resonance (1212 nm), which is well-matched to the wavelength of optimal coupling (1216 nm). In addition, the eight-stage filter is characterized by a 17-nm FWHM and a 190-nm passband (1100 cm^{-1}) with <1.5 dB of ripple.

The higher-order filter resonance near 1450 nm is of poor quality in both LFs due to the nonoptimal coupling at this wavelength. The performance of the eight-stage filter is sufficient, however, for a number of photonic integrated circuit (PIC) Raman and fluorescence applications, including the rejection of background fiber Raman signal that is present when using fiber-attached lasers. For example, since the background Raman signal generated and collected by a single-mode fiber or waveguide scales approximately as nL/A, where n is the index, L is the length, and A is the cross-sectional mode area,[18] a 1-m long fiber would contribute approximately twice the Raman background as a 10-mm long SiN waveguide. Thus, even a filter with 10-dB rejection and extinction would be sufficient.

4 Conclusions

We have demonstrated the successful design and fabrication of broadband DCs and four-stage and eight-stage LFs on a SiN waveguide platform. We describe the mathematical design criteria for maximum LF extinction, as well as optimized asymmetric couplers to achieve the required broadband coupling ratio. The fabrication was performed at AIM photonics, though the design can be adapted to any waveguide platform that supports broadband optical transmission. These filters are an essential component for PIC Raman or fluorescence sensors that are either fiber-coupled to an off-chip source and detector, or with all components fully integrated on-chip. The eight-stage LF is characterized by a 20-dB extinction on resonance, 17-nm FWHM, and

a 190-nm passband (1100 cm^{-1}) with <1.5 dB of ripple. To our knowledge, this passband represents the largest reported for an interferometric waveguide filter.

Subsequent designs of the LFs will be specific to particular pump wavelengths, such as 785, 1064, or 1310 nm that are commonly used for sensing applications. Though the fabrication tolerances become more demanding at shorter wavelengths, the low index contrast and low loss of SiN for these wavelengths should permit successful designs. As foundry-based PIC fabrication continues to improve, we expect higher performance filters that can be modeled in a manner that accounts for the geometrical and index nonuniformities of the fabrication process. Such filters, when integrated with fiber-coupled sensing PICs, will enable inexpensive chip-scale platforms for biological and chemical sensing.

References

1. A. Dhakal et al., "Nanophotonic waveguide enhanced Raman spectroscopy of biological submonolayers," *ACS Photonics* **3**(11), 2141–2149 (2016).
2. A. Dhakal et al., "Evanescent excitation and collection of spontaneous Raman spectra using silicon nitride nanophotonic waveguides," *Opt. Lett.* **39**, 4025–4028 (2014).
3. S. A. Holmstrom et al., "Trace gas Raman spectroscopy using functionalized waveguides," *Optica* **3**, 891–896 (2016).
4. J. Hbner et al., "Integrated optical measurement system for fluorescence spectroscopy in microfluidic channels," *Rev. Sci. Instrum.* **72**(1), 229–233 (2001).
5. R. Bernini et al., "Planar waveguides for fluorescence-based biosensing: optimization and analysis," *IEEE Sens. J.* **6**, 1218–1226 (2006).
6. F. J. Aparicio et al., "Silicon oxynitride waveguides as evanescent-field-based fluorescent biosensors," *J. Phys. D Appl. Phys.* **47**(40), 405401 (2014).
7. F. Xia et al., "Ultra-compact high order ring resonator filters using submicron silicon photonic wires for on-chip optical interconnects," *Opt. Express* **15**, 11934–11941 (2007).
8. W. Bogaerts et al., "Silicon-on-insulator spectral filters fabricated with CMOS technology," *IEEE J. Sel. Top. Quantum Electron.* **16**, 33–44 (2010).
9. L. Chen et al., "Monolithic silicon chip with 10 modulator channels at 25 GBPS and 100-GHZ spacing," *Opt. Express* **19**, B946–B951 (2011).
10. W. Bogaerts et al., "Compact wavelength-selective functions in silicon-on-insulator photonic wires," *IEEE J. Sel. Top. Quantum Electron.* **12**, 1394–1401 (2006).
11. E. S. Magden et al., "Transmissive silicon photonic dichroic filters with spectrally selective waveguides," *Nat. Commun.* **9**, 3009 (2018).
12. A. Ruocco et al., "SOI lattice filters design framework: from functional parameters to layout," in *Proc. Symp. IEEE Photonics Society Benelux*, p. 222 (2013).
13. K. Yamada et al., "Silicon-wire-based ultrasmall lattice filters with wide free spectral ranges," *Opt. Lett.* **28**, 1663–1664 (2003).
14. R. Adar et al., "Adiabatic 3-dB couplers, filters, and multiplexers made with silica waveguides on silicon," *J. Lightwave Technol.* **10**, 46–50 (1992).
15. M. A. Tran, C. Zhang, and J. E. Bowers, "A broadband optical switch based on adiabatic couplers," in *IEEE Photonics Conf. (IPC)*, pp. 755–756 (2016).
16. Z. Lu et al., "Broadband silicon photonic directional coupler using asymmetric-waveguide based phase control," *Opt. Express* **23**, 3795–3808 (2015).

17. T. H. Stievater et al., "Chemical sensors fabricated by a photonic integrated circuit foundry," *Proc. SPIE* **10510**, 105100I (2018).
18. N. L. Thomas et al., "Impact of fundamental thermodynamic fluctuations on light propagating in photonic waveguides made of amorphous materials," *Optica* **5**, 328–336 (2018).

Nathan F. Tyndall is a research chemist with a BS degree in chemistry from the University of Maryland, Baltimore County. He has spent over 2 years at the Naval Research Laboratory designing, fabricating, and characterizing nanophotonic devices, including integrated filters and functionalized Raman systems.

Todd H. Stievater is a research physicist in the Photonics Technology Branch at the US Naval Research Laboratory in Washington, DC. He currently leads research efforts in nanophotonics, nonlinear optics, semiconductor photonics, cold-atom physics, and photonic integration. He is a senior member of the Optical Society of America.

Dmitry A. Kozak received his PhD in electrical engineering from the University of California, Santa Cruz, California, USA, in 2013. From 2013 to 2015, he was an NRC postdoctoral fellow with the US Naval Research Laboratory (NRL). In 2015 to 2016, he was a Karle fellow with NRL. His research interests include fabrication methods, integrated photonics, and materials for optics applications.

Marcel W. Pruessner received his PhD from the University of Maryland, College Park, and is currently a research engineer at the US Naval Research Laboratory in Washington, D.C. His current research interests include nanophotonics, optonanoelectromechanical systems (opto-MEMS/NEMS), and cavity optomechanics.

Scott A. Holmstrom is a professor of physics and engineering physics at the University of Tulsa in Tulsa, Oklahoma, USA. He received his PhD from Australian National University in Canberra, ACT Australia, and has held summer faculty fellowship positions at both the Air Force Research Laboratory in Dayton, Ohio, USA, and the Naval Research Laboratory in Washington, DC, USA. His current research focus is on the development and testing of photonic integrated circuitry for spectroscopy. He is a member of SPIE.

William S. Rabinovich is the head of the Photonic Materials and Devices Section of the Optical Science Division at the US Naval Research Laboratory. He received his BS degree in physics from Stony Brook University and his MS and PhD degrees in physics from Brown University. He has been on the technical staff at the Naval Research Laboratory since 1989.